Reactive magnetron sputtering of tungsten disulfide (WS_{2-x}) films: Influence of deposition parameters on texture, microstructure, and stoichiometry

V. Weiß,[a] S. Seeger, and K. Ellmer[b]
Department Solarenergieforschung, Hahn-Meitner-Institut, Glienicker Straße 100, D-14109 Berlin, Germany

R. Mientus
Opto-Transmitter-Umweltschutz-Technologie e.V., Köpenicker Straße 325b, D-12555 Berlin, Germany

(Received 10 November 2006; accepted 2 February 2007; published online 16 May 2007)

Tungsten disulfide (WS_{2-x}) films ($0.07 \leqslant x \leqslant 0.7$) were prepared by reactive magnetron sputtering from a tungsten target in rare gas/H_2S atmospheres and at substrate temperatures up to 620 °C. The nucleation and growth of the films were investigated by *in situ* energy dispersive x-ray diffraction (EDXRD) and by *ex situ* techniques such as electron microscopy, elastic recoil detection analysis, and x-ray reflectivity. From the EDXRD analysis it was found that the films always nucleate with the (001) planes, i.e., the van der Waals planes, parallel to the substrate surface. For high deposition rates and/or low substrate temperatures a texture crossover from the (001) to the (100) crystallite orientation occurs during the growth. High deposition rates, low substrate temperatures, or low sputtering pressures lead to a significant lattice expansion of the crystallites in the *c* direction (up to 3%). This is most probably caused by a disturbed or turbostratic film growth induced by the energetic bombardment during film deposition. Reflected and neutralized energetic ions (Ar^0,S^0) from the tungsten target and negative ions (S^-) accelerated in the cathode dark space constitute the main sources of the energetic bombardment leading to crystallographic defects. The energy of these particles can be tailored by (i) thermalization between target and substrate in the sputtering gas or (ii) by a reduction of the discharge or target voltage, respectively, by high frequency excitation of the plasma. Films deposited under favorable conditions with respect to low particle energies and at substrate temperatures higher than 200 °C exhibit a significant sulfur deficiency of up to about 5 at. % compared to the stoichiometric composition of WS_2. This is ascribed to an energetic particle bombardment-induced sulfur desorption from the growing films. © *2007 American Institute of Physics*. [DOI: 10.1063/1.2716395]

I. INTRODUCTION

Since about 20 years much attention has been paid to layered transition metal dichalcogenides (TMDCs) such as $Mo(W)S_2$ and $Mo(W)Se_2$.[1] This interest is motivated by their favorable optoelectronic properties such as a band gap energy of 1–2 eV and a high absorption coefficient ($\alpha \approx 10^5$ cm^{-1} for photon energies >2 eV), rendering them candidates for absorber films in thin film solar cells. The TMDC materials were proposed as photovoltaic absorber materials by Tributsch and Bennett[2] and Tributsch[3] nearly 30 years ago. Experiments were performed with natural and synthetic single crystals with electrochemical contacts.[4–6] Efficiencies reaching even 20% were reported for such systems.[7,8]

The so-called van der Waals planes of these materials, consisting of chalcogen atoms, oriented perpendicular to the *c* axis, constitute surfaces without dangling bonds, thus exhibiting a low electronic defect density. Therefore, highest energy conversion efficiencies were obtained with such surfaces. Later, various techniques have been used to prepare thin films of these materials, including sulfurization of tungsten or tungsten oxide films,[9,10] metal organic chemical vapor deposition,[11–14] annealing of metal/chalcogen multilayers,[15] annealing of amorphous and sulfur-rich films, or reactive and nonreactive (magnetron) sputtering.[16–19] Often some kind of surfactant or crystallization promoter, such as sodium, nickel, or cobalt, was used to improve the crystallographic quality and hence the photosensitivity of these films.[19–23] Such promoters were investigated especially with respect to its ability to induce a pronounced (001)-textured film growth, i.e., with the van der Waals planes parallel to the substrate surface. The role of nickel for the crystal growth promotion was demonstrated by Regula *et al.*,[22] who showed that liquid NiS_x droplets dissolve WS_2 and form a supersaturated solution for the liquid-phase growth of large (001)-oriented WS_2 crystallites. However, a quite large amount (some at. %) of nickel (or any other promoter) is needed to observe the required effect. Since NiS_x is a degenerated semiconductor with an almost metal-like conductivity,[24] one has to expect that the photovoltaic properties of a heterojunction solar cells with such absorber films are disturbed by these NiS_x inclusions, for instance, by short circuiting the front and back contacts.[25]

[a]Present adress: Infineon Technologies, Königsbrücker Str. 180, D-01099 Dresden, Germany.
[b]Electronic mail: ellmer@hmi.de

Magnetron sputtering is a versatile low-temperature thin film deposition method that is already used for large-area coatings on architectural and low-emissivity glass. Also for thin film solar cells, magnetron sputtering is used to fabricate metal back (for instance, molybdenum) and transparent oxide front [for instance, indium tin oxide (ITO) or ZnO] contacts. Reactive magnetron sputtering is advantageous since metallic targets can be used, which are cheaper and more robust, than compound targets.

It is the aim of this article to systematically investigate the correlation between deposition and plasma parameters and the structural quality of WS_{2-x} films. For this purpose *in situ* x-ray diffraction at a synchrotron radiation source[26] and *ex situ* methods such as electron microscopy, x-ray reflectivity, and elastic recoil detection analysis have been used. Recently, we have performed a comparable investigation for MoS_{2-x} films.[27] The research on van der Waals- or layer-type semiconductor films is part of a long-term project for the qualification of reactive magnetron sputtering as a deposition method for sulfides (CdS, $CuInS_2$, and In_2S_3) as active layers in thin film solar cells.[28] Recently, we could show that reactive magnetron sputtering from metallic copper and indium targets in Ar/H_2S atmosphere can be used to prepare $CuInS_2$ films of high structural and optoelectronic quality.[29] From such films solar cells with more than 10% efficiency were made, a value which is comparable to solar cells, prepared by pure thermal processing,[30] thus proving the suitability of magnetron sputtering for the deposition of active absorbers in thin film solar cells.

This article is organized in the following way. Section II summarizes the experimental setup, details of which were already described in Ref. 26. The *in situ* x-ray diffraction results and the *ex situ* experiments are presented and discussed in Sec. III. The conclusions are given in Sec. IV. Selected results, especially concerning the influence of the plasma excitation frequency, were already published in a rapid research note.[31]

II. EXPERIMENT

The WS_x films were deposited by reactive magnetron sputtering from a pure tungsten target in argon-H_2S atmospheres. A transportable sputtering and *in situ* x-ray diffraction chamber was used, which has been described recently.[26] The *in situ* experiments were performed at the synchrotron radiation source HASYLAB (DESY-Hamburg, Germany). Details of the deposition system and the diffraction setup are summarized in Tables I and II (see also Ref. 27). Elastic recoil detection analysis (ERDA) with heavy ions (Kr, Xe, and Au) with energies of 1.8 MeV/amu was used to measure the chemical composition of the films with a sensitivity limit of about 0.01 at. %.[32]

From the tungsten WL_α x-ray fluorescence intensities, measured during the *in situ* analysis (see Sec. III A 1), the atomic areal density $N_\square$ [at. cm^{-2}] of tungsten defined as

TABLE I. Parameters of the deposition system.

Target (purity)	W (99.95%)
Target diameter	51 mm
Target-to-substrate distance	60 mm
Sputtering gases (purity)	Ar (5*N*), H_2S (99.5%)
Base pressure	1×10^{-4} Pa
Plasma excitation	dc, rf (13.56 or 27.12 MHz)
Sputtering pressure	0.5–9 Pa
Flow ratio $F_{H_2S}/(F_{H_2S}+F_{Ar})$	0–1.0
Substrate temperature	200–620 °C
Substrates	(100) silicon/oxidized (>100 nm)

$$N_\square = \frac{N_A d_f \rho_{\text{film}}}{M_W} \tag{1}$$

was calculated by a calibration with films of known atomic areal density, measured by ERDA, since this method directly yields the atomic areal density $N_\square$ (see Ref. 32). In Eq. (1) d_f and ρ_{film} are the thickness and the density of the film and M_W is the atomic mass of tungsten.

Scanning electron microscopy (SEM) was performed with a Hitachi S-4100 field emission microscope (electron energy of 25 keV). A Philips CM12 transmission electron microscope (TEM) (LaB_6 cathode, 120 keV) was used to analyze the cross-sectional samples, which were prepared by standard mechanical and ion beam thinning techniques.

All film thicknesses were measured with a surface profilometer (DEKTAK 3030, Veeco) at film steps generated by scratching. Additionally, the density, the thickness, and the surface roughness of very thin films ($d_f<80$ nm) were obtained from grazing incidence x-ray reflectivity (GIXR) measurements with Cu $K\alpha$ radiation (Siemens D5000).

III. RESULTS AND DISCUSSION

A. *In situ* x-ray diffraction analysis

1. Time-resolved x-ray diffraction

Figure 1(a) shows a typical series of energy dispensive x-ray diffraction (EDXRD) spectra measured during the deposition of a (001)-textured WS_{2-x} film by dc sputtering. Besides the weak fluorescence lines $WL_{\alpha,\beta}$ strong diffraction signals of the (002), (004), and (006) lattice planes of the hexagonal $2H$-WS_2 (Ref. 46) phase can be seen at the beginning of the film growth. The diffraction peaks increase fast in intensity, slowing down the further the deposition progresses. Phases other than the $2H$-WS_2 and the metallic tungsten phase were not observed in our experiments.

It is already visible at a first glance from Fig. 1(a) that the (002) peak occurs from the very beginning of the depo-

TABLE II. Parameters of the diffraction setup.

Diffraction angle	4.5°
Size of primary beam	100 μm(W)×300 μm(H)
Photon energy	7–60 keV
Energetic resolution	>220 eV
Measurement time/spectrum	20–30 s
Fluorescence lines	$WL_{\alpha,\beta}$ (8.40 and 9.67 keV)

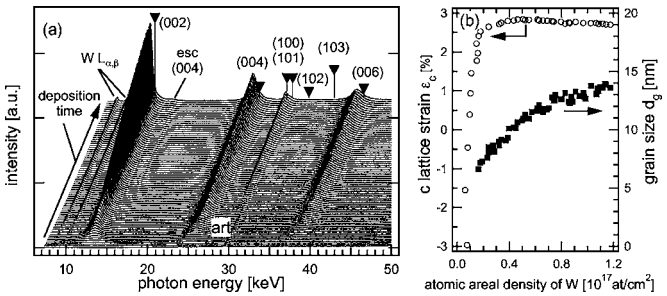

FIG. 1. (a) EDXRD-spectra series during magnetron sputtering (dc excitation) of a WS_{2-x} film on an oxidized (100) silicon substrate. The vertical bars with triangles indicate position and intensity of the powder diffraction pattern of 2H-WS_2 (Ref. 46). The escape signal (esc) is due to the detection system and occurs at an energy of 9.9 keV (Ge Kα fluorescence energy) smaller than the " (004)-mother peak." An electronic artifact (art) occurs at 29.5 keV. Deposition parameters: Total deposition time 40 min, sputtering power 50 W_{dc}, gas flow ratio $F_{H_2S}/(F_{Ar}+F_{H_2S})=0.75$, sputtering pressure 9 Pa, substrate temperature 450 °C, substrate bias −25 V (floating potential), stoichiometry $WS_{1.93}$, and total film thickness 110 nm. (b) Lattice strain in the *c*-direction (○) and grain size d_g (■) in dependence on the tungsten atomic areal density.

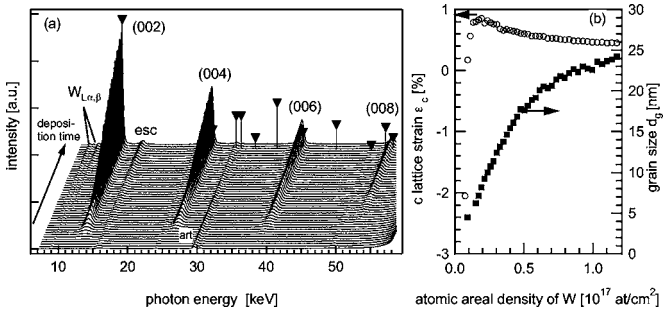

FIG. 2. (a) EDXRD-spectra series during magnetron sputtering (rf-27 MHz excitation) of a WS_{2-x} film on an oxidized (100) silicon substrate. Deposition parameters: Total deposition time 30 min, sputtering power 50 W_{rf}, gas flow ratio $F_{H_2S}/(F_{Ar}+F_{H_2S})=0.75$, sputtering pressure 2 Pa, substrate temperature 620 °C, substrate bias 18 V (floating potential), stoichiometry $WS_{1.81}$, and total film thickness 70 nm. (b) Lattice strain in the *c* direction (○) and grain size d_g (■) in dependence on the tungsten atomic areal density. Other data see Fig. 1.

sition. This means that the nucleation of the WS_{2-x} films occurs with the van der Waals planes parallel to the substrate surface and was observed under all deposition conditions. After about 15 min deposition time a small, asymmetric broad peak rises at an energy of about 29 keV which can be attributed to the combined (100)/(101) peak of 2*H*-WS_2. This means that the original (001)-textured film growth (*c*-axis perpendicular to the substrate, $c_\perp$) is disturbed and starts to switch to the growth of (100)-oriented crystallites, i.e., to grains with its *c* axes parallel to the substrate surface ($c_\parallel$).

The widths of the diffraction peaks show a strong decrease during the film growth. This is reflected in the grain size d_g, calculated from the peak widths[26] and depicted in Fig. 1(b). A continuous grain growth up to a grain size (coherently diffracting regions) of 14 nm can be observed, which saturates when (100)-oriented grains start to grow. Comparing the measured diffraction peak positions with the corresponding data of a WS_2 powder [JCPDS, see the bars with triangles in Fig. 1(a)], a significant shift can be observed. From the energetic positions of the (002) diffraction signals the *c*-lattice strain ε_c of the lattice cell of 2*H*-WS_2 was calculated $[\varepsilon_c=(c_{\text{film}}-c_{\text{powder}})/c_{\text{powder}}]$, which is also shown in Fig. 1(b). The lattice strain in the *c* direction shows a characteristic behavior with a strong increase from negative values of about −3% to positive values as large as 3% followed by a small reduction. The smaller *c*-lattice constant (negative ε_c) at the beginning of the film growth could be explained by the strong bonding of the S–W–S layer to the silicon dioxide. It could also be possible that the bonding between SiO_2 and the film occurs directly by O–W bonds, which are stronger than S–W bonds, leading to a lower lattice constant at the beginning of the film growth. After some layers (about three, corresponding to 1×10^{16} at. cm^{-2}) have been deposited, the *c* axis develops towards its equilibrium value ($\varepsilon_c\approx0$). Further film growth leads to a significant expansion of the distance of the S–W–S layer ($\varepsilon_c\approx3\%$). This is, however, not caused by mechanical stress, which was checked by profilometric measurements of coated silicon cantilevers; mechanical stress would also not fit with the low yield strength and hardness of layer-type materials such as graphite or molybdenum and tungsten disulfide. Instead, it is plausible that the lattice expansion is due to the formation of a large number of crystallographic defects, especially dislocations. This can be inferred from the occurrence of crystallites with (100) orientation which can be imagined to nucleate at crystallographic defects (see Ref. 33). Also TEM cross-sectional pictures prove the high defect density (see Sec. III B). The slight decrease of ε_c at higher thickness points to some self-annealing of the defects.

Figure 2(a) shows a comparable series of EDXRD spectra for a WS_{2-x} film, deposited by rf magnetron sputtering with an excitation frequency of 27.12 MHz. At this high frequency the discharge voltage (absolute value) is reduced from about 500 V (dc) to 80 V (rf) and hence the deposition rate decreases significantly. By comparison with Fig. 1 it is obvious that the crystallographic quality of the rf-sputtered film has improved considerably. In the EDXRD spectra the (100)-oriented grains are absent, pointing to a lower defect density during growth, explained in more detail below. The better crystallographic quality can also be elucidated from the larger grain sizes and from the *c*-axis deformation [see Fig. 2(b)] which is lower by a factor of about 6. The thickness dependence of the *c*-lattice deformation is qualitatively comparable to that of the film deposited by dc sputtering. However, the relaxation after the maximum lattice expansion is more pronounced for the rf-sputtered film, which seems to be plausible taking into account a lower defect density.

Since the comparison of these two films was done for the same discharge power, i.e., at different deposition rates due to the different discharge (target) voltages, we performed also a comparison of two films deposited at 12 W (dc) and 50 W (rf-27 MHz) which was done for the same deposition rate (≈2.4 nm/min), displayed in Fig. 3. Again, it is obvious that the dc sputtering leads to a worse crystallographic film quality compared to the rf sputtering. This means that the deposition rate is not the decisive parameter for the structural quality of the sputtered films. The strong influence of the excitation frequency, i.e., the discharge voltage, was already

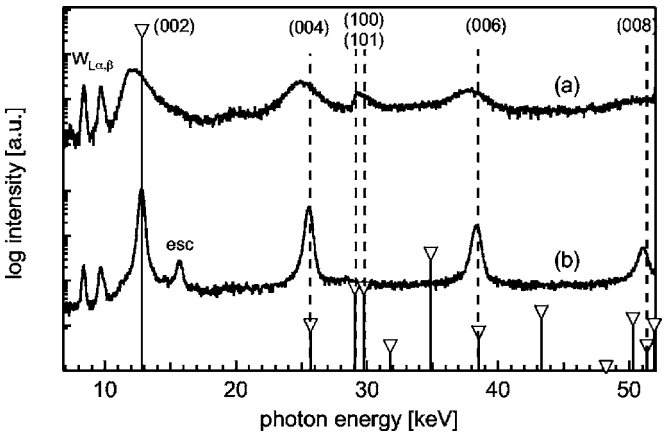

FIG. 3. Comparison of EDXRD spectra (logarithmic scale) of two WS_{2-x} films on oxidized (100) silicon substrates deposited by (a) 12 W (dc) and (b) 50 W (rf-27 MHz) plasma excitation, yielding the same deposition rates. Deposition parameters: Gas flow ratio $F_{H_2S}/(F_{Ar}+F_{H_2S})=0.75$, sputtering pressure 2 Pa, substrate temperature 450 °C, substrate bias (floating potential) −5 V (dc), 14.5 V (rf), stoichiometry $WS_{1.84}$ (rf), and total film thicknesses 190 nm (dc), 100 nm (rf).

shown recently by us.[31] Therefore, we can conclude that the energy of the species (see the different discharge voltages) contributing to the film growth, i.e., sputtered atoms, ions traversing the plasma sheath in front of the substrate, energetic atoms, reflected and neutralized at the target surface, and negative sulfur ions accelerated across the plasma sheath in front of the target, influences significantly the film growth and the crystallographic perfection of the WS_{2-x} films.

2. Pressure and substrate temperature dependence for dc plasma excitation

In order to further prove the argument of the influence of the energy of the particles contributing to film growth, the sputtering pressure was varied by more than one order of magnitude. It is well known that by collisions of species from the target surface with the sputtering gas thermalization occurs.[34] Depositions performed at sputtering pressures between 0.5 and 9 Pa are compared in Fig. 4(a) by means of the (002) peak area in dependence on the areal density of tungsten atoms (at. cm^{-2}), i.e., the deposited amount of tungsten atoms which was derived from the WL_α fluorescence peak area. All (002) signal areas, except that of the deposition at 9 Pa, show a steep increase at the beginning, reach a maximum, and decrease at a larger film thickness. The decrease can be assigned to two effects. (i) The film growth of (001)-oriented crystallites stops at about 1×10^{17} W at. cm^{-2} (corresponding to a film thickness of 18 nm, assuming stoichiometric WS_2 and bulk density) and is followed by the (100) growth mode. (ii) Self-absorption of the x rays diffracted at (001)-oriented crystallites in that part of the film growing above the (001)-oriented grains.

The dependence of the peak area A_{002} on the thickness d can be fitted by the following expression:

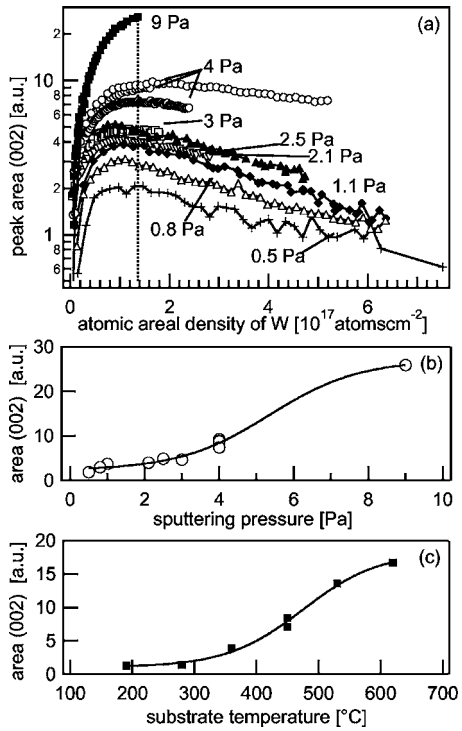

FIG. 4. (a) Development of the peak area of the (002) diffraction signals vs the atomic areal density of tungsten (as a measure of the film thickness) during WS_{2-x} depositions at different sputtering pressures. Deposition parameters: Sputtering power 50 W_{dc}, gas flow ratio $F_{H_2S}/(F_{Ar}+F_{H_2S})=0.75$, substrate temperature 450 °C, and floating substrate potential. Normalized saturation values (at a constant atomic areal density of 1.37×10^{17} W at. cm^{-2}) in dependence on the deposition parameters sputtering pressure (b) and substrate temperature (c). Deposition parameters: Sputtering power 50 W_{dc}, gas flow ratio $F_{H_2S}/(F_{Ar}+F_{H_2S})=0.75$, sputtering pressure 4 Pa, and floating substrate potential.

$$A_{hkl}=A_{\mathrm{sat}}\left\{1-\exp\left[-\left(\frac{d}{d_{\mathrm{cryst}}}\right)^{n}\right]\right\}\exp\left(-\frac{\mu\rho d}{\sin\theta}\right), \qquad (2)$$

which takes into account both effects. The first part of Eq. (2) is a Johnson-Mehl-Avrami expression[35] where A_{sat} is the saturation peak area after the texture crossover from the (001) to the (100) growth mode. The crystallization thickness d_{cryst} marks the film thickness at which the first (002) grains can be detected by XRD. The Johnson-Mehl-Avrami reaction order n adopts values from 1 to 4, depending on the crystallization process investigated. According to Humphreys and Hatherly,[35] n exhibits values between 1 and 2 for two-dimensional film growth. The second part of the equation is a standard absorption relationship taking into account the x-ray absorption coefficient μ of WS_2 (8365 $cm^2\ g^{-1}$), the density ρ (bulk WS_2 value: 7.73 g cm^{-3}) of the growing film, and the diffraction angle θ.

The fact that self-absorption of the (002) diffraction signal was observed for the film deposition of WS_{2-x} but not in the case of MoS_{2-x} films[27] can be explained by the higher absorption coefficient of WS_2 (i.e., the attenuation length is smaller by a factor of 15!). The fit of the thickness (or time) dependent peak areas by Eq. (2) leads to crystallization thicknesses d_{cryst} of about 70 nm and a reaction order of about 1.2, corresponding to two-dimensional growth with completed nucleation.

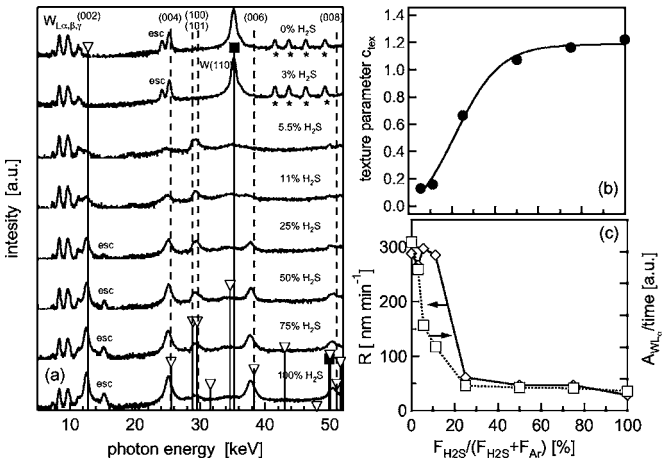

FIG. 5. (a) A series of EDXRD spectra of WS_{2-x} films deposited on oxidized (100) silicon substrates at gas flow ratios $F_{H_2S}/(F_{Ar}+F_{H_2S})$ from 0% to 100%. (b) Texture parameter c_{tex} in dependence on the gas flow ratio $F_{H_2S}/(F_{Ar}+F_{H_2S})$ for the spectra from Fig. 5(a). (c) Deposition rates R measured by profilometry ($\diamond$) and derived from the WL_α fluorescence peaks in relative units ($\square$) in dependence on the gas flow ratio $F_{H_2S}/(F_{Ar}+F_{H_2S})$. The vertical bars with triangles and squares indicate position and intensity of the powder diffraction patterns of 2*H*-WS_2 (Ref. 46) and tungsten (Ref. 47). Deposition parameters: Total deposition time 6 (0% H_2S) to 30 (100% H_2S) min, sputtering power 100 W_{rf}, sputtering pressure 2 Pa, substrate temperature 620 °C, and substrate bias (floating potential) 8 V (0% H_2S) to 20 V (100% H_2S).

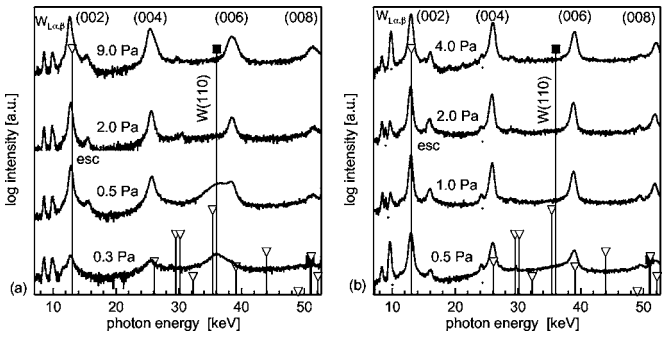

FIG. 6. Series of EDXRD spectra of WS_{2-x} films deposited on oxidized (100) silicon for different total sputtering pressures and two sputtering powers of 100 W_{rf} (a) and 50 W_{rf} (b). Deposition conditions: Gas flow ratio $F_{H_2S}/(F_{Ar}+F_{H_2S})=0.75$, substrate temperature 620 °C, substrate bias 17 V (floating potential), and stoichiometry $WS_{1.95}$ (100 W), $WS_{1.81}$ (50 W). Other data see Fig. 5.

The saturation values A_{sat} of the (002) peak depend on pressure and temperature. Figure 4(b) shows the increase of A_{sat}, i.e., the volume of coherently scattering (001)-oriented crystallites, with increasing sputtering pressure. It can be seen that the A_{sat} values increase with the sputtering pressure, which is caused by two effects: a decreasing deposition rate, due to gas scattering and a reduced energy of energetic particles, due to thermalization at the sputtering gas atoms.

The observed temperature dependence of this (002) saturation peak area is given in Fig. 4(c). At higher temperatures a less disturbed growth of (001)-oriented crystallites and therefore higher (002) peak areas can be seen. This can be explained by a higher mobility of the deposited atoms at the film surface which leads to a higher crystallographic order.

3. Influence of the H_2S-to-Ar ratio

The effect of the reactive component H_2S in the sputtering atmosphere is not obvious *a priori*. Since it contains an oxidizing (S) as well as a reducing component (H) it is not clear whether the required sulfurization really occurs. Therefore, a deposition series was performed in which the relative amount of H_2S in the sputtering atmosphere was varied from 0% to 100%. The EDXRD spectra at the end of the depositions are compared in Fig. 5. At low H_2S contents in the sputtering gas the films are tungsten rich, visible from the strong W(110) diffraction peak at 35.5 keV, accompanied by a regular peak pattern (∗) above a photon energy of 40 keV, which is caused by the high count rate of the W(110) peak (electronic overmodulation of the Ge detector).

The tungsten disulfide phase can be observed already at a H_2S portion of 5.5% in the sputtering atmosphere; however, these films exhibit a (100)/(101) texture. For a gas flow ratio $F_{H_2S}/(F_{H_2S}+F_{Ar})$ of 25% the films grow with a clear (001) texture while the amount of (100)-oriented crystallites stays constant. From the ratio of the (002) and the (100/(101) diffraction peaks the texture parameter c_{tex} was calculated as

$$c_{tex} = \frac{A_{(002)}}{A_{(002)}+A_{(100/101)}} \frac{I^{JCPDS}_{(002)}+I^{JCPDS}_{(100/101)}}{I^{JCPDS}_{(002)}}, \quad (3)$$

which is normalized to the intensity ratio of the powder diffraction file (Ref. 46). From Fig. 5(b) it can be seen that the (001) texture increases significantly for H_2S portions of 50% or more. This is caused by the abruptly decreasing deposition rate [about a factor of 6, see Fig. 5(c)], which was derived from the WL_α fluorescence peak area and independently measured by profilometry. It has to be noted that both rates deviate significantly from each other for H_2S contents between 5% and 20%, which we interpret as due to a significant reduction of the density of such films since the profilometric rate is significantly higher than the (relative) rate derived from the tungsten fluorescence (see also Sec. III C). For $F_{H_2S}/(F_{H_2S}+F_{Ar})$ ratios larger than 25% the (001) texture of the WS_{2-x} films becomes more pronounced mainly caused by the increase of the (00l) diffraction peaks, while the combined (100)/(101) peak of WS_2 is nearly constant. However, this improvement of the texture cannot be ascribed to a variation of the deposition rate, since it stays constant [Fig. 5(c)]. Instead, we think that additional sulfur in the sputtering atmosphere leads to a better repair of sulfur vacancies which are induced by energetic particle bombardment. This can be inferred also from a slightly increasing sulfur content of the films (see Fig. 11). Also, such sulfur vacancies are nucleation seeds for WS_2 crystallites growing in the (100)/(101) orientation, making it plausible that with increasing partial pressure of sulfur, i.e., decreasing sulfur vacancy concentration, the (001) texture improves. Nevertheless, it has to be stated that even in a pure hydrogen sulfide atmosphere the films exhibit a stoichiometry of only about 1.9 (see Sec. III D), which could be caused by the high atomic hydrogen content of the magnetron plasma, leading to a much more pronounced reducing effect, compared to a thermal H_2S treatment.

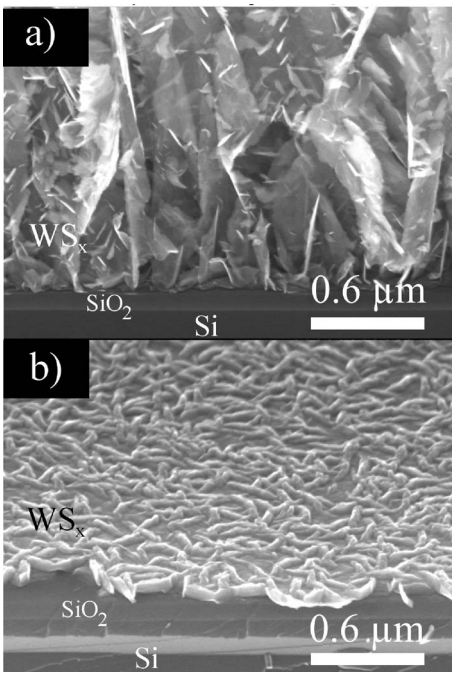

FIG. 7. Cross-sectional SEM pictures from the depositions performed at the lowest (a) and at the highest (b) rate. Deposition parameters: Sputtering power 50 W_{dc}, gas flow ratio $F_{H_2S}/(F_{Ar}+F_{H_2S})=0.2$ (a) and 0.75 (b), sputtering pressure 4 Pa, substrate temperature 450 °C, and floating substrate potential.

4. Pressure dependence for rf plasma excitation

The role of particle bombardment during WS_{2-x} film growth was investigated also for 27 MHz excitation by varying the sputtering pressure from 0.5 to 9 Pa for a fixed flow ratio $F_{H_2S}/(F_{H_2S}+F_{Ar})=0.75$. In Fig. 6 two series of EDXRD spectra are displayed, measured during depositions at sputtering powers of 100 and 50 W to about the same film thickness, visible from the WL_α fluorescence peak intensities. At high pressure, for both discharge powers strongly (001)-textured films are grown. Decreasing the sputtering pressure below about 1 Pa leads to a less (001)-textured growth and to the formation of a new peak at about 35.5 keV, which can be attributed to the (110)-tungsten diffraction peak. This means that the increased particle energies at low pressures (less thermalization in the sputtering gas) induce a sulfur deficiency in the films accompanied by the growth of tungsten nanocrystallites, which can be inferred from the broad (110)-W diffraction peaks. This sulfur deficiency was also detected by ERDA, see Sec. III D. The effect of the bombardment by energetic particles is much more pronounced for the deposition at 100 W, due to the higher discharge voltage (140 V).

B. Scanning and transmission electron microscopy (SEM/TEM)

Figure 7 displays SEM micrographs of two films deposited at a high (a) and a low (b) deposition rate. The film morphology changes significantly from a highly porous, dendritic film growth at high rates to relatively flat, compact films at a low deposition rate. The EDXRD spectra reveal that the compact, flat films exhibit a pronounced (001) texture, while the porous films experienced a texture crossover from the (001) to the combined (100)/(101) texture. The film density measurements (see Sec. III C) confirm the SEM observations and yield nearly the bulk density for film (b) and a density of only about 25% of the bulk density for film (a). The occurrence of the (100)-oriented crystallites leads to a very porous film structure, which cannot be "switched back" to the (001) texture, for instance, by changing the growth conditions (low rate, high pressure, and high temperature). This is due to the fact that the growth rate of the (100)-oriented crystallites (growth perpendicular to the c axis) is much higher (about a factor of 5) compared to the growth along the c axis.[36,37]

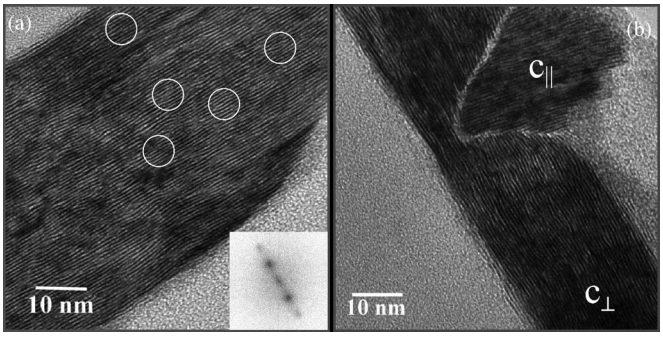

FIG. 8. XTEM micrographs of a WS_{2-x} film on oxidized silicon. (a) A film with a $c_\perp$-oriented basal layer; the white circles mark different crystallographic defects. (b) A film region, where a $c_\parallel$-oriented crystallite grows out of a $c_\perp$-oriented basal layer. Inset: two-dimensional Fourier analysis picture. Deposition parameters: Sputtering power 50 W_{dc}, gas flow ratio $F_{H_2S}/(F_{Ar}+F_{H_2S})=0.75$, sputtering pressure 4 Pa, substrate temperatures 620 °C (a) and 450 °C (b); floating substrate potential −30 V, and stoichiometry $WS_{1.74}$.

Cross-sectional TEM (XTEM) micrographs were prepared in order to study the atomic structure of the films (Fig. 8). These pictures show resolved S–W–S planes (black lines) in the (001) orientation ($c_\perp$) at the interface WS_{2-x}/SiO_2. After a certain thickness has been reached, crystallites growing perpendicular to the thin nucleation layer can be observed ($c_\parallel$).

The d_{002} value, i.e., the distance of the S–W–S layers, was analyzed by a two-dimensional Fourier transformation of selected areas of the XTEM micrographs and yielded lattice parameters $d_{002}=c/2$ between 0.65 and 0.67 nm, which confirm the lattice expansion in the c direction of several percent measured by the EDXRD experiments (JCPDS: $d_{002}=0.6181$ nm). Careful inspection of the XTEM pictures reveals a large number of crystallographic defects, mostly dislocations, visible as bifurcations and inserted short lattice planes of S–W–S layers (black lines). In Fig. 8(a), such defects are marked by different white circles. On the basis of the high resolution TEM pictures a dislocation density of about 3×10^{12} cm^{-2} was estimated by counting the edge dislocations in a Fourier filtered TEM picture of the $c_\perp$-oriented basal layer. About the same value was determined recently for our MoS_{2-x} films.[27]

C. Film density

From the measured atomic areal density $N_\square$ [at. cm^{-2}] (ERDA) and the measured profilometric film thickness d_f the film density can be calculated according to

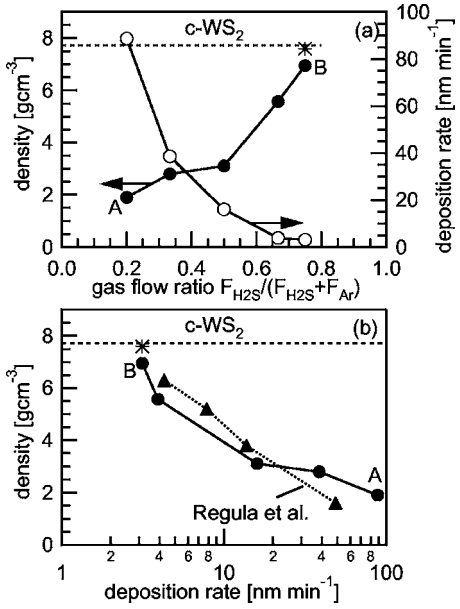

FIG. 9. (a) Density (●) and deposition rate (○) of reactively sputtered WS_{2-x} thin films on oxidized silicon substrates obtained from ERDA measurements in dependence on the gas flow ratio $F_{H_2S}/(F_{H_2S}+F_{Ar})$. The horizontal line marks the density of a WS_2 single crystal (7.73 g cm^{-3}). The star (⋆) displays the density of one sample also measured by x-ray reflectometry. The capital letters in the diagram refer to the cross-sectional SEM images of these samples shown in Fig. 7. In diagram (b) the rate dependence of the film density is plotted on a semilogarithmic scale. The results from Regula *et al.* (Ref. 38) are given for comparison (▲). Deposition parameters: dc sputtering power 50 W, substrate temperature 450 °C, total sputtering pressure 4 Pa, and floating substrate potential.

$$\rho_{\text{film}} = N_{\square}\frac{\sum [x_i]M_i}{N_A d_f}, \tag{4}$$

with N_A, the Avogadro number; M_i, the atomic masses; and $[x_i]$ the relative portion of atom i. The film densities are depicted in Fig. 9(a) in dependence on the gas flow ratio. Low H_2S partial pressures lead to very porous films with densities of as low as 25% of the density of a WS_2 single crystal (x-ray density: 7.73 g cm^{-3}). At a H_2S content of 75% in the gas mixture the x-ray density of WS_2 is almost reached. This thin, compact film (thickness of about 50 nm) could be analyzed independently by x-ray reflectometry (*), which confirmed the value derived from ERDA and thickness measurements. The porous morphology of WS_x films, which was confirmed by the SEM analysis (corresponding to points A and B, see Fig. 7), results from dendritic structures that are typical for layer-type materials prepared at high deposition rates and which were reported by other groups, too.[38] The deposition rate strongly depends on the H_2S partial pressure, depicted in Fig. 9(a), and itself influences the density of the growing films. In Fig. 9(b) the dependence of the density on the deposition rate is plotted in order to compare the results with the literature data of Regula *et al.*[38] Both series fit well against each other although these authors used diode sputtering characterized by much higher discharge voltages (1350–1700 V) compared to magnetron sputtering, used by us, with discharge voltages between about 500 V (dc) and 80 V (rf). Also, their sputtering conditions were different from ours: a WS_2 compound target, only

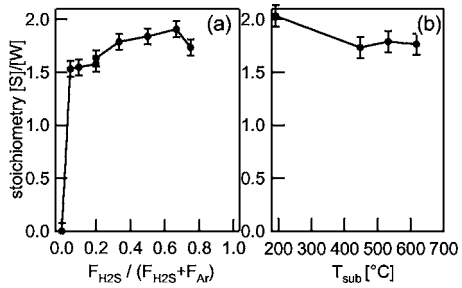

FIG. 10. Stoichiometry [S]/[W] of reactively dc-sputtered WS_{2-x} films on oxidized silicon substrates in dependence on the gas flow ratio $F_{H_2S}/(F_{Ar}+F_{H_2S})$ (a) and in dependence on the substrate temperature (b). Deposition parameters: dc sputtering power 50 W, total sputtering pressure 4 Pa, floating substrate potential, substrate temperature 450 °C (a) and gas flow ratio $F_{H_2S}/(F_{H_2S}+F_{Ar})=0.75$ (b).

1% H_2S in the sputtering gas and the deposition rate, was varied via the total sputtering pressure (1–6 Pa). The good agreement of the density versus deposition rate curves indicates similar growth modes for both deposition processes with respect to the film density. For the (001)-oriented grain structure which leads to dense, compact films, a low growth rate is essential, i.e., a high sulfur content in the sputtering atmosphere accompanied by a low sulfur vacancy concentration in the films. At high deposition rates the partial pressure of sulfur seems to be no longer sufficient to avoid sulfur vacancies in the growing film, which constitute nucleation sites for the growth of (100)-oriented crystallites inducing a porous film morphology.

D. Stoichiometry

The stoichiometries, i.e., the sulfur-to-tungsten ratios [S]/[W] of the films, calculated from the ERD data, yield sulfur-deficient films ([S]/[W]<2.0) for substrate temperatures >200 °C. This is comparable to MoS_{2-x} films reported recently.[27]

Figures 10(a) and 10(b) show the stoichiometries of WS_{2-x} films in dependence on the gas flow ratio and the substrate temperature. Increasing the partial pressure of H_2S leads to an increase of the sulfur content up to [S]/[W] =1.91. The decrease of the stoichiometry for the highest gas flow ratio $F_{H_2S}/(F_{H_2S}+F_{Ar})=0.75$ [see Fig. 10(a)] was probably caused by an oxygen contamination of the films due to a leak of the sputtering chamber during this specific deposition, which was detected only afterwards. Of the contaminations found in the films, oxygen and hydrogen are the most prominent ones with concentrations up to 9 at. %. The other contaminations—nitrogen and argon—are lower than 1 at. %. The total amount of the contaminations detected in the films does not account for the large deviations (up to 20%) from the composition WS_2. With decreasing argon gas flow the concentration of the hydrogen and carbon contaminations also decreases which is a hint that the argon gas supply or tubing may be the origin of this contamination. The high oxygen concentrations in the films are difficult to assign only to the WS_x films as the films were deposited onto oxidized silicon. Therefore, the separation between oxygen in the film and oxygen from the SiO_2 is only possible with an

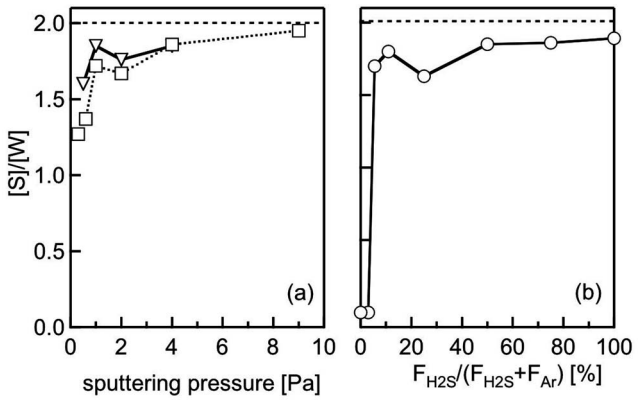

FIG. 11. Stoichiometry [S]/[W] of reactively rf-sputtered WS_{2-x} thin films on oxidized silicon substrates in dependence on the sputtering pressure (a) and the gas flow ratio $F_{H_2S}/(F_{Ar}+F_{H_2S})$ (b). Deposition parameters: rf-27 MHz sputtering power 50 W, floating substrate potential, substrate temperature 620 °C, gas flow ratio $F_{H_2S}/(F_{H2}S+F_A)=0.75$ (a), and total sputtering pressure 4 Pa (b).

error of ±20%. The argon concentrations in the films are only slightly above the detection limit of 0.1 at. %.

Figure 10(b) shows the film stoichiometry in dependence on the substrate temperature. As already mentioned stoichiometric WS_2 can only be prepared at temperatures below 200 °C, which, however, has a nearly amorphous structure. The decrease of the sulfur content in the films with increasing temperature is explained for MoS_{2-x} with an increased vapor pressure of sulfur that desorbs from the substrate prior to the reaction to the sulfide,[39] which is also plausible for WS_{2-x} films.

The range of sulfur-to-tungsten ratios found in our experiments is in agreement with results from other groups.[38] As shown above, there are strong indications from the structural investigations (TEM and XRD) that this sulfur deficiency is connected with structural imperfections of the WS_2 lattice. Owing to the low bonding forces between the van der Waals (001)-lattice planes,[40] the crystallographic order in the *c* direction is disturbed, leading to a so-called turbostratic growth, accompanied by a sulfur deficiency in the van der Waals planes. Another fact that could cause a sulfur deficiency is the quite high amount of reactive, i.e., atomic hydrogen, which is formed in the plasma from the reactive sputtering gas H_2S, leading to a reduction of the growing WS_2 film to WS_{2-x}. This argument could be used to explain the dependence of the [S]/[W] ratio versus the flow ratio $F_{H_2S}/(F_{H_2S}+F_{Ar})$, displayed in Fig. 11(b). Here it can be seen that the sulfur content of the films increases continuously with increasing H_2S partial pressure, but it is not reaching a value of 2.0. The same can be found for the variation of the sputtering pressure, depicted in Fig. 11(a). In both figures, a drop of the [S]/[W] ratio at a sputtering pressure of 2 Pa and a flow ratio of 25%, respectively, is visible, which can be ascribed to the throttling of the pumping speed with the help of the main gate valve. This means that the flow velocity of the H_2S influences the reaction of the H_2S at the substrate surface.

The presented results show that a significant improvement of the crystallographic film quality can be achieved by decreasing the energies of the plasma species at the substrate surface using rf excitation, high substrate temperature, and a high sputtering pressure. Nevertheless, the prepared films are sulfur deficient and exhibit a poor electronic quality,[41] rendering it unsuitable for absorbers in thin film solar cells. This high sensitivity of WS_2 (and also MoS_2, see Ref. 27) against energetic particle bombardment is in strong contrast to recent results on reactive magnetron sputtering of $CuInS_2$ absorbers for thin film solar cells[29] in our group or for magnetron sputtering of CdTe films by Gupta and Compaan.[42] The reason for this striking difference is firstly the higher defect formation energies (some eV at least) in these covalently bonded compound semiconductors. A second reason seems to be that these semiconductors are quite defect tolerant, which makes them much more radiation resistant than Si or GaAs, for instance, for use in solar cells on satellites.[43]

On the other hand, the transition metal dichalcogenides, such as $MoS(Se)_2$ or $WS(Se)_2$, are characterized by weak van der Waals-like bonds along its *c* axis with bonding energies of the order of only 0.15 eV between two sulfur atoms in MoS_2, calculated recently by Rydberg *et al.*[40] This leads to a higher defect density of these materials in an ion-assisted deposition process such as reactive magnetron sputtering. Therefore, other preparation routes, for instance, metal-promoted crystallization from amorphous, sulfur-rich precursors (MoS_{3+x}, WS_{3+x}) by (rapid) thermal annealing,[18,25,41,44,45] are more promising than direct plasma-assisted deposition methods.

IV. CONCLUSIONS

In situ x-ray diffraction was used to systematically investigate the nucleation and the growth of tungsten disulfide films (WS_{2-x}) deposited by reactive magnetron sputtering.

(i) Under all deposition conditions investigated with respect to pressure, substrate temperature, deposition rate, and plasma excitation frequency, the films start to grow in the (001) orientation, i.e., with the van der Waals planes parallel to the substrate surface.

(ii) Depending on the deposition rate, the deposition pressure, and the plasma excitation frequency a texture crossover occurs from the (001) to the (100) orientation of the crystallites. This behavior is comparable to that of the structurally equivalent molybdenum disulfide films, which were investigated recently.[27]

(iii) The film growth is strongly influenced by the plasma excitation frequency which was varied from 0 Hz (dc) to 27.12 MHz. Caused by the decreasing discharge (target) voltage with increasing excitation frequency the lattice expansion $\Delta c/c$ is significantly reduced, which can be explained by a lower crystallographic defect density.

(iv) The composition of the WS_{2-x} films was determined by elastic recoil detection analysis. Only for a substrate temperature of 200 °C a sulfur-to-tungsten ratio of 2.0 (i.e., $x=0$) was found. For higher substrate temperatures a sulfur deficiency up to 5 at. % (i.e., $x=0.1$) was observed. This sulfur deficiency was tentatively ascribed to the bombardment of the growing

film by energetic species, leading to a particle-induced desorption of sulfur. Species contributing to this effect are reflected argon or sulfur atoms and, especially, negative sulfur ions, accelerated in the cathode dark space to the highest energy available in the deposition system.

(v) The electrical analysis of the films shows that the high defect density, even of the best films with respect to the crystallographic data, leads to poor electronic film quality, i.e., the films are not photoactive.[41] This can be attributed to the weak binding between the S–W–S planes (0.15 eV) (Ref. 40) in WS_2, which is much lower compared to covalently bonded semiconductors such as silicon, gallium arsenide, or chalcopyrites.

Taking together all observations, it is doubtful if direct reactive magnetron sputtering can be used to prepare WS_2 absorber films for thin film solar cells.

ACKNOWLEDGMENTS

We thank W. Bohne, J. Röhrich, E. Strub, and S. Lindner from the Ion Beam Laboratory (ISL) of our Institute who performed the ERD analysis. H. Wulff and M. Quaas (Ernst-Moritz-Arndt University, Greifswald) are acknowledged for the x-ray reflectivity analysis. Last but not the least we are grateful to Ulrike Bloeck and Ina Sieber who made the cross-sectional samples and the TEM pictures and the SEM analysis, respectively.

[1] *Photoelectrochemistry and Photovoltaics of Layered Semiconductors*, edited by A. Aruchamy (Kluwer Academic, Dordrecht, 1992).
[2] H. Tributsch and J. C. Bennett, J. Electroanal. Chem. Interfacial Electrochem. **81**, 97 (1977).
[3] H. Tributsch, Ber. Bunsenges. Phys. Chem. **81**, 362 (1977).
[4] H. Tributsch, Sol. Energy Mater. **1**, 257 (1979).
[5] C. R. Cabrera and H. D. Abruna, J. Electrochem. Soc. **135**, 1436 (1988).
[6] W. Jaegermann and H. Tributsch, Prog. Surf. Sci. **29**, 1 (1988).
[7] R. Tenne and A. Wold, Appl. Phys. Lett. **47**, 707 (1985).
[8] C. Azaiez, F. Lévy, G. Campet, and J. Claverie, in Sixth International Conference on Photochemical Conversion Storage Solar Energy, Paris, France, 1986, p. D-54.
[9] A. Ennaoui, S. Fiechter, K. Ellmer, R. Scheer, and K. Diesner, Thin Solid Films **261**, 124 (1995).
[10] E. Galun *et al.*, Appl. Phys. Lett. **67**, 3474 (1995).
[11] G. Chatzitheodorou, S. Fiechter, M. Kunst, J. Luck, and H. Tributsch, Mater. Res. Bull. **23**, 1261 (1988).
[12] W. K. Hofmann, J. Mater. Sci. **23**, 3981 (1988).
[13] S. Tiefenbacher, H. Sehnert, C. Pettenkofer, and W. Jaegermann, Surf. Sci. Lett. **318**, L1161 (1994).
[14] J.-W. Chung, Z. R. Dai, and F. S. Ohuchi, J. Cryst. Growth **186**, 137 (1998).
[15] J. Ouerfelli, J. C. Bernede, A. Khelil, and J. Pouzet, Appl. Surf. Sci. **120**, 1 (1997).
[16] J. Pouzet and J. C. Bernede, Mater. Chem. Phys. **36**, 304 (1994).
[17] M. Regula, C. Ballif, and F. Lévy, in *Polycrystalline Semiconductors IV*, edited by S. Pizzini, H. P. Strunk, and J. H. Werner (Trans Tech, Zug, Switzerland, 1995), pp. 335–340.
[18] C. Ballif, M. Regula, P. E. Schmid, M. Remskar, R. Sanjines, and F. Lévy, Appl. Phys. A: Mater. Sci. Process. **62**, 543 (1996).
[19] K. Ellmer, C. Stock, K. Diesner, and I. Sieber, J. Cryst. Growth **182**, 389 (1997).
[20] G. Salitra, G. Hodes, E. Klein, and R. Tenne, Thin Solid Films **245**, 180 (1994).
[21] A. Matthäus *et al.*, J. Electrochem. Soc. **144**, 1013 (1996).
[22] M. Regula, C. Ballif, M. Remskar, and F. Lévy, J. Vac. Sci. Technol. A **15**, 2323 (1997).
[23] E. A. Ponomarev, R. Tenne, A. Katty, and C. Lévy-Clement, Sol. Energy Mater. Sol. Cells **52**, 125 (1998).
[24] D. J. Vaughan and J. R. Craig, *Mineral Chemistry of Metal Sulfides* (Cambridge University Press, Cambridge, 1978).
[25] C. Ballif, M. Regula, and F. Lévy, Sol. Energy Mater. Sol. Cells **57**, 189 (1999).
[26] K. Ellmer, R. Mientus, V. Weiß, and H. Rossner, Meas. Sci. Technol. **14**, 336 (2003).
[27] V. Weiß *et al.*, J. Appl. Phys. **95**, 7665 (2004).
[28] L. Gawallek, C. Salzmann, J. Klaer, J. Bruns, M. Kanis, and K. Ellmer, in Second World Conference and Exhibit on Photovoltaic Solar Energy Conversion, edited by J. Schmid, H. A. Ossenbrink, P. Helm, H. Ehmann, and E. D. Dunlop, Vienna, Austria, 6–10 July 1998 (EU Joint Research Center), pp. 553–556.
[29] T. Unold, I. Sieber, and K. Ellmer, Appl. Phys. Lett. **88**, 213502 (2006).
[30] K. Siemer, J. Klaer, I. Luck, J. Bruns, R. Klenk, and D. Bräunig, Sol. Energy Mater. Sol. Cells **67**, 159 (2001).
[31] K. Ellmer, R. Mientus, S. Seeger, and V. Weiß, Phys. Status Solidi A **201**, R97 (2004).
[32] W. Bohne, J. Röhrich, and G. Röschert, Nucl. Instrum. Methods Phys. Res. B **136–138**, 633 (1998).
[33] J. Moser and F. Lévy, J. Mater. Res. **7**, 734 (1992).
[34] G. M. Turner, J. Vac. Sci. Technol. A **13**, 2161 (1995).
[35] F. J. Humphreys and M. Hatherly, *Recrystallization and Related Annealing Phenomena* (Pergamon, Oxford, 1995).
[36] M. K. Agarwal, K. N. Reddy, and H. B. Patel, J. Cryst. Growth **46**, 139 (1979).
[37] F. Pedraza, J. Cruz-Reyes, D. Acosta, M. J. Yanez, M. Avalos-Borja, and S. Fuentes, J. Phys.: Condens. Matter **5**, A219 (1993).
[38] M. Regula, C. Ballif, J. H. Moser, and F. Lévy, Thin Solid Films **280**, 67 (1996).
[39] T. Ito and K. Nakajima, Philos. Mag. B **37**, 773 (1978).
[40] H. Rydberg, M. Dion, N. Jacobson, E. Schröder, P. Hyldgaard, S. I. Simak, D. C. Langreth, and B. I. Lundqvist, Phys. Rev. Lett. **91**, 126402 (2003).
[41] S. Seeger, S. Brunken, R. Kunst, R. Mientus, and K. Ellmer (to be submitted).
[42] A. Gupta and A. D. Compaan, Appl. Phys. Lett. **84**, 684 (2004).
[43] A. Jasenek, H. W. Schock, J. H. Werner, and U. Rau, Appl. Phys. Lett. **79**, 2922 (2001).
[44] O. Lignier, G. Couturier, and J. Salardenne, J. Appl. Phys. **82**, 6110 (1997).
[45] K. Ellmer, S. Seeger, and R. Mientus, Phys. Status Solidi A **203**, 2457 (2006).
[46] Joint Committee on Powder Diffraction Standards Card No. 8-237, International Center for Diffraction Data, Newton Square, PA (2001).
[47] Joint Committee on Powder Diffraction Standards Card No. 4-806, International Center for Diffraction Data, Newton Square, PA (2001).